Numerical study of a turbulent co-axial non-premixed flame for methanol hydrothermal combustion

Comparison of the EDC and FGM models

Ren, Mengmeng; Wang, Shuzhong; Romero-Anton, N.; Zhao, Junxue; Zou, Chong; Roekaerts, Dirk

DOI
10.1016/j.supflu.2020.105132

Publication date
2021

Document Version
Accepted author manuscript

Published in
Journal of Supercritical Fluids

Numerical study of a turbulent co-axial non-premixed flame for methanol hydrothermal combustion: comparison of the EDC and FGM models

Mengmeng Ren[a,*], Shuzhong Wang[b], N. Romero-Anton[c], Junxue Zhao[a], Chong Zou[a], Dirk Roekaerts[d,*]

[a] School of Metallurgical Engineering, Xi'an University of Architecture and Technology, Xi'an 710055, China

[b] Key Laboratory of Thermo-Fluid Science and Engineering of MOE, School of Energy and Power Engineering, Xi'an Jiaotong University, Xi'an 710049, China

[c]ENEDI Research Group, Faculty of Engineering in Bilbao, University of the Basque Country UPV/EHU, Plaza Torres Quevedo 1, 48013, Bilbao, Spain

[d] Department of Process and Energy, Delft University of Technology, Leeghwaterstraat 39, 2628 CB Delft, The Netherlands

*Corresponding Author.

Email address: ren.meng.meng@163.com (M. Ren); D.J.E.M.Roekaerts@tudelft.nl (D. Roekaerts).

Abstract

Eddy dissipation concept (EDC) model and flamelet generated manifolds (FGM) model are developed separately to study the temperature profiles and extinction limits of non-premixed hydrothermal flames. Predictions by the two models are evaluated comparatively by experimental data in literatures. FGM model shows relatively better prediction of temperature than EDC model in the near nozzle field. Extinction temperatures can be predicted by EDC model with deviations of 10 K to 33 K. The extinction flow rates predicted by the FGM model are higher than those by the EDC model. Flow fields and reaction source terms are analysed to identify the inherent mechanism leading different results by the two models. It is illustrated that the positive effect of turbulence on reaction rate near the nozzle by the FGM model is the essential reason causing different flame characteristics from the EDC model by which the turbulence only has negative effect on reaction rate.

Keywords

Hydrothermal combustion; Eddy dissipation concept (EDC) model; Flamelet generated manifolds (FGM) model; Flame temperature profile; Extinction limits; Turbulence-chemistry interaction

1 Introduction

Hydrothermal combustion refers to the rapid oxidation reaction occurring in a supercritical water environment [1]. Supercritical water, due to its good solvent and transport properties, is an ideal medium for various chemical processes, such as hydrothermal gasification [2, 3], liquefaction [4, 5], synthesis [6, 7] and oxidation [8-10]. A hydrothermal flame serves as an internal heat source for these processes. For endothermic processes, for example hydrothermal gasification, the hydrothermal flame provides the needed heat [11]. For exothermic processes, for example Supercritical water oxidation (SCWO) which is a promising wet waste treatment technology, the hydrothermal flame can promote the complete degradation of the organic waste and optimize the energy recovery of the system [12, 13].

Developing reliable numerical methods to investigate the flow and reaction mechanism of the hydrothermal combustion is of great importance for the design and optimization of the best flame configuration in various processes. Narayanan et al. [14] have used the eddy dissipation (ED) model to simulate the hydrothermal flame in the ETH (Swiss Federal Institute of Technology) wall-cooled hydrothermal burner (WCHB). The eddy dissipation (ED) model assumes that the chemical reaction rate is far faster than the turbulent mixing rate and then the combustion reaction rate is equal to the turbulent mixing rate. Based on the eddy-dissipation model, Sierra-Pallares et al.

[15] developed the multiple-time-scale (ED-MTS) turbulent mixing model to calculate the mixing rate considering the large Schmidt number in supercritical fluids. However, these models are not accurate for conditions where the chemical reaction rate is comparable to the mixing rate. Queiroz et al. [16] have simulated a turbulent hydrothermal flame in a vessel reactor. They have pointed out that at low injection temperature the chemical reaction rate is slower than the mixing rate, and therefore adopted the laminar finite-rate (FR) model with a one-step reaction mechanism. In our previous study [17], the eddy-dissipation/finite-rate (ED/FR) model was used to simulate the ETH hydrothermal flame, in which the combustion reaction rate is taken as the smaller one between the one-step chemical reaction rate and the turbulent mixing rate. By including finite-rate effects the extinction limit could be studied using the ED/FR model but was found to be underpredicted by 150 K due to the inaccurate representation of the turbulence-chemistry interaction.

In order to describe chemical effects such as ignition and extinction accurately detailed chemical reaction kinetics is needed [18-20]. In hydrothermal conditions, special attention should be paid to the real-fluid thermodynamic and transport properties. In the case of turbulent flow the kinetic model has to be integrated in a model for turbulence-chemistry interaction (TCI). In this work we have chosen to work with two different TCI model which are meant to be used in combination with detailed kinetics, namely the eddy dissipation concept (EDC) model [21-23] and the flamelet generated manifolds (FGM) model [24-26]. Both are widely used but belong to different class of models. The EDC model introduces a model for the turbulence chemistry interaction in which the reactions take place in a fine structure of the flow which evolves kinetically as plug flow or well-stirred reactor. The EDC model is relatively easier to implement the real-fluid properties through a commercial software

as ANSYS Fluent, but recent work [21, 27] on MILD combustion indicate that the EDC model may produce significant discrepancies due to the strong turbulence-chemistry interaction at the diluted condition. The hydrothermal combustion condition is also highly diluted by supercritical water, so the performance of the EDC model at hydrothermal condition is in suspense. The FGM model belongs to the subset of the flamelet-based models, which represent the local flame structure as having properties of pre-computed laminar flames. In the FGM model, the independent variables of mixture fraction and progress variable are resolved together to extend the limit of the basic flamelet model that only thin flames can be modelled accurately. A known superiority of the FGM model over the EDC model is the better computational efficiency. The question will be addressed which of the two approaches is performing best for turbulent hydrothermal flames. The application of FGM in turbulent hydrothermal combustion can build upon our previous work on laminar counterflow methanol hydrothermal combustion [28]. Here the laminar methanol FGM tables will be extended to include the influence of turbulent fluctuations. Numerical model development needed to reach this goal includes implementation of real fluid thermodynamic and transport properties in CHEM1D (laminar flame code) and the link between the generated FGM tables and the turbulent flame code ANSYS Fluent.

In this work both the EDC model and the FGM model are applied to simulate the turbulent diffusion flames of methanol hydrothermal combustion in the ETH combustor configuration [29, 30]. The predicted temperature contours by the two models are compared, as well as the key scalars and flow field are analysed to reveal the underlying flow and reaction mechanism. To illustrate the inherent difference between the two models, comparative analysis of the turbulence-chemistry

interactions by the two models is conducted by explicitly turning off the turbulence effect on reaction rate. In the end, the abilities of the two models to predict the extinction limits are evaluated from the view of extinction temperature and extinction mass flow rate.

2 Model and method

2.1 Governing Equations

To describe the flow and reaction process in turbulent hydrothermal combustion, we use the Reynolds-averaged governing equations [31]. These include the mean continuity equation, the mean momentum equation, the mean species transport equations and the mean energy equation.

$$\frac{\partial \overline{\rho}}{\partial t}+\frac{\partial\left(\overline{\rho}\tilde{u}_i\right)}{\partial x_i}=0 \tag{1}$$

$$\frac{\partial\left(\overline{\rho}\tilde{u}_j\right)}{\partial t}+\frac{\partial\left(\overline{\rho}\tilde{u}_i\tilde{u}_j\right)}{\partial x_i}=-\frac{\partial \overline{p}}{\partial x_j}+\frac{\partial \overline{\tau}_{ij}}{\partial x_i}-\frac{\partial}{\partial x_i}(\widetilde{\overline{\rho}u_i"u_j"}) \tag{2}$$

$$\frac{\partial\left(\overline{\rho}\tilde{Y}_k\right)}{\partial t}+\frac{\partial\left(\overline{\rho}\tilde{u}_i\tilde{Y}_k\right)}{\partial x_i}=\frac{\partial}{\partial x_i}\left(\overline{\rho}\overline{D}\frac{\partial \tilde{Y}_k}{\partial x_i}\right)+\overline{\dot{\omega}}_k-\frac{\partial}{\partial x_i}\left(\widetilde{\overline{\rho}u_i"Y_k"}\right) \tag{3}$$

$$\frac{\partial\left(\overline{\rho}\tilde{h}\right)}{\partial t}+\frac{\partial\left(\overline{\rho}\tilde{u}_i\tilde{h}\right)}{\partial x_i}=\frac{\partial}{\partial x_i}\left(\overline{\lambda}\frac{\partial \tilde{T}}{\partial x_i}\right)-\frac{\partial}{\partial x_i}\left(\widetilde{\overline{\rho}u_i"h"}\right). \tag{4}$$

where ρ、u_i、p、τ_{ij}、Y_k、D、$\dot{\omega}_k$、h、λ and T respectively denote density, velocity, pressure, viscous stress, mass fraction of species *k*, mass diffusion coefficient, production rate of species *k*, specific enthalpy, thermal conductivity and temperature. The overbar denotes the Reynolds-averaged value, while the tilde denotes the density weighted or Favre-averaged value. To any variable *f*, the relation

between the Reynolds-averaged value and the Favre-averaged value is $\overline{\rho}\tilde{f} = \overline{\rho f}$, while the primed quantities are defined by $f = \overline{f} + f' = \tilde{f} + f''$.

In the above governing equations, major closure problems are present in the Reynolds stress $\widetilde{u_i''u_j''}$, the turbulent flux of mass fraction $\widetilde{u_i''Y_k''}$ and enthalpy $\widetilde{u_i''h''}$, and the mean reaction source term $\overline{\dot{\omega}}_k$. For the Reynolds stress term, the standard k-ε model is adopted as:

$$\overline{\rho}\widetilde{u_i''u_j''} = \mu_t\left(\frac{\partial\tilde{u}_i}{\partial x_j} + \frac{\partial\tilde{u}_j}{\partial x_i}\right) - \frac{2}{3}\left(\overline{\rho}k + \mu_t\frac{\partial\tilde{u}_k}{\partial x_k}\right)\delta_{ij} \tag{5}$$

where $\mu_t = \overline{\rho}C_\mu\dfrac{k^2}{\varepsilon}$ is the turbulent viscosity. k and ε are the turbulence kinetic energy and its dissipation rate. k and ε are closed by their transport equations:

$$\frac{\partial\left(\overline{\rho}k\right)}{\partial t} + \frac{\partial\left(\overline{\rho}\tilde{u}_i k\right)}{\partial x_i} = \frac{\partial}{\partial x_i}\left(\left(\mu + \frac{\mu_t}{\sigma_k}\right)\frac{\partial k}{\partial x_i}\right) + G_k - \overline{\rho}\varepsilon \tag{6}$$

$$\frac{\partial\left(\overline{\rho}\varepsilon\right)}{\partial t} + \frac{\partial\left(\overline{\rho}\tilde{u}_i\varepsilon\right)}{\partial x_i} = \frac{\partial}{\partial x_i}\left(\left(\mu + \frac{\mu_t}{\sigma_\varepsilon}\right)\frac{\partial\varepsilon}{\partial x_i}\right) + C_{1\varepsilon}\frac{\varepsilon}{k}G_k - C_{2\varepsilon}\overline{\rho}\frac{\varepsilon^2}{k} \tag{7}$$

$$G_k = -\overline{\rho}\widetilde{u_i''u_j''}\frac{\partial\tilde{u}_j}{\partial x_i} \tag{8}$$

where C_μ, $C_{1\varepsilon}$ and $C_{2\varepsilon}$ are constants 0.09, 1.44 and 1.92. σ_k and σ_ε are Prandtl numbers with default values of 1 and 1.3.

The turbulent fluxes are closed by the classical gradient diffusion assumption:

$$\overline{\rho}\widetilde{u_i''Y_k''} = -\frac{\mu_t}{Sc_t}\frac{\partial\tilde{Y}_k}{\partial x_i} \tag{9}$$

$$\overline{\rho}\widetilde{u_i''h''} = -\frac{\mu_t}{\sigma_t}\frac{\partial\tilde{h}}{\partial x_i} \tag{10}$$

where Sc_t and σ_t are the turbulent Schmidt number and the Prandtl number with default values of 0.7 and 0.85. Due to the analogous forms, the turbulent fluxes are always combined with the diffusion terms in the transport equations, presenting the enhancement of diffusion by turbulence. Some closure problems are also present in the mean transport coefficients (viscosity, mass diffusivity and thermal conductivity) but these terms are relatively small compared to the main ones in highly turbulent flow and are evaluated at the mean temperature and composition.

2.2 Closure of the turbulent reaction source term

The key problem in turbulent combustion simulation is the closure of the mean reaction source term. The reaction source term is a highly nonlinear function of temperature and species concentrations:

$$\dot{\omega}_k = \sum_i^{Nr} (n''_{i,k} - n'_{i,k}) A_i T^{\beta_i} e^{\frac{-E_i}{RT}} \prod_j^{Ns} [C_j]^{n'_{i,j}} \tag{11}$$

where N_r is the number of reactions and N_s is the number of species , A_i, β_i and E_i are the pre-exponential factor, the temperature exponent and the activation energy of the i-th reaction, $[C_j]$ is the concentration of species j, $n'_{i,k}$ and $n'_{i,j}$ are the stoichiometric coefficients for species k and j as reactants in the i-th reaction, $n''_{i,k}$ is the stoichiometric coefficient for species k as product in the i-th reaction. The mean reaction source term is not equal to the instantaneous reaction rate evaluated using mean temperature and mean concentrations. In this work we shall use two different closures of the mean source term, the EDC model and the FGM model with presumed PDF of which the details will be descried in the following sections. In both models, the detailed chemical mechanism of methanol hydrothermal combustion developed by our previous work [32] is applied, which contains 23 species and 103 reactions. It was

developed from on a gas-phase combustion mechanism [33] by modifying the pressure-dependent and hydrothermal sensitive reactions.

2.2.1 The eddy dissipation concept (EDC) model

The eddy dissipation concept (EDC) model belongs to the class of closure models presuming a subdivision of the volume in small reaction structures and surrounding nonreacting environment. The detailed definition involves quantification of the relative size of the reacting structures, the way the reaction proceeds and how fast the mass transfer is with the surroundings. The length scale ξ^* and time scale τ^* of the reacting structures are of dependent on the turbulent kinetic energy and its dissipation rate:

$$\xi^* = C_\xi \left(\frac{\nu\varepsilon}{k^2} \right)^{1/4} \tag{12}$$

$$\tau^* = C_\tau \left(\frac{\nu}{\varepsilon} \right)^{1/2} \tag{13}$$

Here ν is the kinematic viscosity and C_ξ and C_τ are model constants with default values of 2.1377 and 0.4082. The scaling is based on the assumption that the reacting structures are of the size of the Kolmogorov scale. The model combines a purely chemical component and a pure mixing component. The local fine structure is considered to be a constant pressure reactor and the thermochemical state reached after evolution according to the chemical mechanism from the current value $\tilde{Y}_i$ over a time scale τ^* is denoted as Y_i^*. The mean reaction rate describes a relaxation from the current state $\tilde{Y}_i$ to Y_i^* according to mixing time scale also determined by the volume fraction of reacting structures:

$$\bar{\dot{\omega}}_k = \frac{\bar{\rho}\left(\xi^*\right)^2}{\tau^*\left[1-\left(\xi^*\right)^3\right]}\left(Y_i^* - \tilde{Y}_i\right) \tag{14}$$

2.2.2 The flamelet generated manifolds (FGM) model

The FGM model assumes that the local state in the flame is a set canonical flames described by just a few independent variables. These states are stored in look-up tables that are used in the calculation of the flame to be investigated. In this work, the methanol hydrothermal FGM tables generated by counterflow flames are used, which have been generated and evaluated thoroughly in our previous research [28]. They are dependent on two independent variables, mixture fraction Z and progress variable Y_c. Mixture fraction Z stands for the elemental mass fraction that originated from the fuel side. Here the Bilger's formation [34] is adopted which considers the effect of differential diffusion:

$$Z = \frac{2M_H^{-1}[Y_H - Y_{H,2}] + 0.5M_C^{-1}[Y_C - Y_{C,2}] - M_O^{-1}[Y_O - Y_{O,2}]}{2M_H^{-1}[Y_{H,1} - Y_{H,2}] + 0.5M_C^{-1}[Y_{C,1} - Y_{C,2}] - M_O^{-1}[Y_{O,1} - Y_{O,2}]} \tag{15}$$

where M_H, M_C, M_O is the molar mass of element *H, C, O*. Z_H, Z_C, Z_O is the mass fraction of element *H, C, O*. $Z_{H,1}$, $Z_{C,1}$, $Z_{O,1}$ is the mass fraction of element *H, C, O* at the fuel side and $Z_{H,2}$, $Z_{C,2}$, $Z_{O,2}$ is the mass fraction of element *H, C, O* at the oxidizer side. The definition of Y_c has been optimized as function of mass fraction of CO_2 [28]. The influence of turbulence on the mean reaction rate can then be described by the joint probability density function of these two variables. Assuming statistical independence of mixture fraction and a scaled progress variable c, defined as $c = (Y_c - Y_{c,\min}(Z)) / (Y_{c,\max} - Y_{c,\min}(Z))$, the joint probability density function can be written as product of two marginal distribution functions P_Z and P_c. The marginal distribution functions have an assumed form (β-function) fully characterised by

mean and variance. Then the mean of any local thermochemical quantity can be obtained from

$$\widetilde{\Phi} = \widetilde{\Phi}(\tilde{Z}, \widetilde{Z''^2}, \tilde{c}, \widetilde{c''^2}) = \int \int \Phi(Z,c) P(Z;\tilde{Z}, \widetilde{Z''^2}) P(c;\tilde{c}, \widetilde{c''^2}) \, dZ \, dc \tag{16}$$

Where $\tilde{Z}$, $\widetilde{Z''^2}$, $\tilde{c}$, $\widetilde{c''^2}$ denote the mean mixture fraction, the variance of the mixture fraction, the normalized progress variable, the variance of the progress variable. $\widetilde{\Phi}$ represents any local variable including temperature, species mass fraction, density, heat capacity etc., as well as the source term of progress variable:

$$\widetilde{S_{Y_c}} = \frac{\overline{\dot{\omega}}_c}{\overline{\rho}} = \int \int S_{Y_c}(Z,c) P(Z,\tilde{Z}, \widetilde{Z''^2}) P(c,\tilde{c}, \widetilde{c''^2}) \, dZ \, dc \tag{17}$$

The mean values are stored in the four-dimensional FGM tables with mean and variance of mixture fraction and progress variable as independent parameters.

Instead of mean transport equations of species, the following mean transport equations of Z and Y_c are solved

$$\frac{\partial\left(\overline{\rho}\tilde{Z}\right)}{\partial t} + \frac{\partial\left(\overline{\rho}\tilde{u}_i\tilde{Z}\right)}{\partial x_i} = \frac{\partial}{\partial x_i}\left(\left(\frac{\overline{\lambda}}{\overline{C}_{\mathrm{p}}} + \frac{\mu_{\mathrm{t}}}{\sigma_{\mathrm{t}}}\right)\frac{\partial\tilde{Z}}{\partial x_i}\right) \tag{18}$$

$$\frac{\partial\left(\overline{\rho}\tilde{Y}_c\right)}{\partial t} + \frac{\partial\left(\overline{\rho}\tilde{u}_i\tilde{Y}_c\right)}{\partial x_i} = \frac{\partial}{\partial x_i}\left(\left(\frac{\overline{\lambda}}{\overline{C}_{\mathrm{p}}} + \frac{\mu_{\mathrm{t}}}{Sc_{\mathrm{t}}}\right)\frac{\partial\tilde{Y}_{\mathrm{c}}}{\partial x_i}\right) + \overline{\dot{\omega}}_c \tag{19}$$

The transport equations of the variance of mixture fraction and progress variable are also solved:

$$\frac{\partial\left(\overline{\rho}\widetilde{Z''^2}\right)}{\partial t} + \frac{\partial\left(\overline{\rho}\tilde{u}_i\widetilde{Z''^2}\right)}{\partial x_i} = \frac{\partial}{\partial x_i}\left(\left(\frac{\overline{\lambda}}{\overline{C}_{\mathrm{p}}} + \frac{\mu_{\mathrm{t}}}{\sigma_{\mathrm{t}}}\right)\frac{\partial\widetilde{Z''^2}}{\partial x_i}\right) + C_{\mathrm{g}}\mu_{\mathrm{t}}\left(\frac{\partial\tilde{Z}}{\partial x_i}\right)^2 - C_{\mathrm{d}}\overline{\rho}\frac{\varepsilon}{k}\widetilde{Z''^2} \tag{20}$$

$$\frac{\partial\left(\overline{\rho}\widetilde{Y_c''^2}\right)}{\partial t} + \frac{\partial\left(\overline{\rho}\tilde{u}_i\widetilde{Y_c''^2}\right)}{\partial x_i} = \frac{\partial}{\partial x_i}\left(\left(\frac{\overline{\lambda}}{\overline{C}_{\mathrm{p}}} + \frac{\mu_{\mathrm{t}}}{Sc_{\mathrm{t}}}\right)\frac{\partial\widetilde{Y_c''^2}}{\partial x_i}\right) + C_\phi\frac{\mu_{\mathrm{t}}}{Sc_{\mathrm{t}}}\left(\frac{\partial\tilde{Y}_c}{\partial x_i}\right)^2 - C_\phi\overline{\rho}\frac{\varepsilon}{k}\widetilde{Y_c''^2}$$

(21)

where $C_{g,z}$ $C_{d,z}$ C_{g,Y_c} C_{d,Y_c} are model constants with values of 2.86, 2.0, 2.0 and 2.0. In this way, the transport of species is described by only four transport equations, which significantly reduces the computational effort.

2.3 Computational setup

The ETH hydrothermal reactors are cylindrical in shape with injection of fuel (methanol and water) from the exit of a pipe aligned with the axis and injection of oxygen in the same direction from an annular slit close to the wall [29, 30]. Experiments have been done with two reactors of different size, referred to as WCHB-II [29] and the WCHB-III [30], here respectively used to validate the modelling results of the extinction temperature and the axial temperature profile. The fuel injector diameter and the inner and outer diameter of the annular slit for oxygen injection of WCHB-II and WCHB-III are respectively 1.5/7/9 mm and 1.6/6/8.5 mm. As done in previous simulations of this type of burners [14, 15], the computational domain is chosen as 2D axi-symmetric. The domain is bounded in radial direction by the inner wall of the combustion chamber and the domain extends in axial direction from 10 mm upstream of the outlet of the fuel pipe exit until 100 mm downstream.

The default model settings for a RANS simulation are used in ANSYS Fluent, apart from the thermodynamic and transport properties, which are set to those of supercritical conditions. For the EDC model, after importing the detailed chemistry kinetic mechanism, the properties at pressure of 25 MPa including density, heat capacity, thermal conductivity and viscosity of main species are represented as piecewise-linear functions of temperature. For the FGM model, the hydrothermal FGM tables of laminar counterflow flames are generated by a modified version of CHEM1D which considers the non-ideal thermodynamic and transport properties of

supercritical fluids [28], and from the resulting laminar FGM a table of mean values is obtained by the laminar values with the beta function PDF's for mixture fraction and progress variable to get the FGM-PDF tables with mean and variance of mixture fraction and mean and variance of scaled progress variable as independent variables as explained in Section 2.2.2. The generated FGM-PDF tables are read by a user defined function (UDF) DEFINE_PDF_TABLE which makes available the tabulated flame state variable needed in the solution of the governing equations. It needs to be pointed out that the definition of progress variable Y_c has been slightly changed compared to what was done in the laminar flame studies of Ref. [28]. Because the upper limit of Y_c is required to be 1 in ANSYS Fluent, here Y_c is defined as equal to the mass fraction of CO_2 instead of mass fraction divided by molar mass. It should be pointed out that the FGM table is generated from adiabatic laminar flames which induces some limitations in the representation of the experimental conditions with wall kept at constant temperature by an external cooling system. In order to take into account non-adiabatic effects, it would be necessary to extend the tabulation with enthalpy as an extra independent variable. Huang et al. [35] listed several methods to do so. Most simply by considering the effect of enthalpy loss only on the temperature while retaining the species mass fraction as adiabatic, or more correctly via heat loss in the laminar flame calculations, either in the boundary condition [36] or via a source term in the energy equation [37, 38]. This generalisation has not yet been developed for the hydrothermal flame case and therefore the discussion in the results section will mainly focus on the adiabatic case.

Geometry and operating conditions of the cases computed in this work are collected in Table 1. They are distinguished by different methanol concentration in the fuel w_f, fuel inlet temperature T_f and mass flow rate m_f, oxygen inlet temperature

T_o and mass flow rate m_o, the wall condition and the geometry. Case 1~2 will be used to analyse the model prediction on the temperature profiles. Case 3~5 enable the study of the extinction temperatures at fixed fuel concentration and mass flow rate. Case 6~7 enable study of the extinction mass flow rate at fixed fuel concentration and inlet temperature.

Table 1 Geometry and operation conditions

Case	w_f(wt%)	T_f(K)	m_f(g/s)	T_o(K)	m_o(g/s)	Wall condition	Geometry
1	16	700	1.97	700	0.55	T_{wall}=700 K	WCHB-III
2	24	530	1.53	590	0.65	Adiabatic	WCHB-II
3	16	550-650	1.55	580	0.45	T_{wall}=700 K	WCHB-II
4	20	410-510	1.55	569	0.55	T_{wall}=700 K	WCHB-II
5	24	300-450	1.55	571	0.65	T_{wall}=700 K	WCHB-II
6	24	530	1.53-153	590	0.65-65	adiabatic	WCHB-II
7	24	450	1.55-15.5	571	0.65-6.5	adiabatic	WCHB-II

3 Results and discussion

3.1 Temperature profiles

Most research on hydrothermal flames focuses on the ignition and extinction characteristics [29, 30, 39-41] while the spatial temperature profiles of stable flames are seldomly measured. Until now, only the temperature profiles along the combustor axis at supercritical inlet temperature in the WCHB-III are available to validate the simulation results for temperature. It should be pointed out that considering that the temperature is detected by a thermocouple with the diameter of 1mm in the work of Prikopsky [30], a spatial accuracy of ±0.5 mm should be taken into account in the comparisons. Fig. 1 (a) presents the predicted profiles along the axis of the combustor by the EDC and FGM model for case 1, as well as the experimental data from [30]. This case has 16 wt% methanol in water as fuel and pure oxygen as oxidizer with the inlet temperature and wall temperature 700 K. It can be seen that the two models predict nearly identical rapid increase in temperature, while the experimental data

presents an earlier start and more gradual increase of temperature with distance from the nozzle. For axial positions with x>0.04 mm, the results from the two models are clearly different. This difference is due to the different treatments of the energy equation by the two models. The EDC model solves the energy equation and the heat loss by convective heat transfer to the 700 K wall is taken in to account. In the adiabatic FGM model used here, the temperature is determined as a function of the local mixture fraction, progress variable and their variances and the energy equation is not solved. Therefore, the heat loss associated with the constant temperature boundary condition is actually ignored during the FGM modelling. Hence the present FGM model for hydrothermal flames can only predict the adiabatic conditions. Nevertheless it is of interest to see how the predictions of the FGM and EDC can differ in the region close to the nozzle where the nonadiabatic effect is weak. This is explored in Fig. 1 (b). It shows the comparison of the predicted temperature profiles at the off-axis radial position of y=0.5 mm. As mentioned, the experimental temperature measurement has a spatial inaccuracy of 0.5 mm and could also be representing off axis data. It is observed that the result by the FGM model differ a lot by making the 0.5 mm displacement in the radial direction, while that by the EDC model are almost unchanged. Interestingly, the temperature profile predicted by the FGM model agrees well with the experimental temperature rise curve. More experimental data are needed to judge the accuracy of the models, but the present results do show that the FGM model predicts a higher temperature gradient in radial direction.

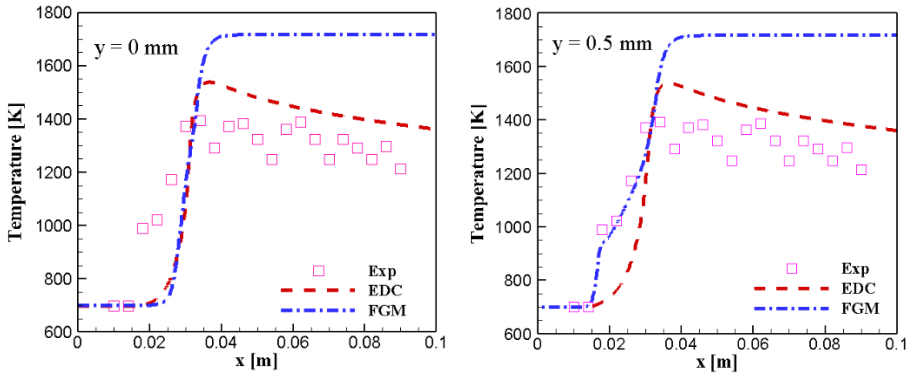

(a) y=0 mm (b) y=0.5 mm

Fig. 1 Axial profiles of mean temperature: predictions by EDC and FGM and experimental measurements (w_f=16 wt%, T_f=700 K)

To be able to really compare the predictions of EDC and FGM, the following sections will only discuss the adiabatic conditions. Fig. 2 shows the comparison of the temperature contours predicted by the two models at the adiabatic condition of 530 K 24 wt% methanol as fuel and 590 K pure oxygen as oxidizer. It is clear that at this condition the flame location and the flame thickness predicted by the FGM model and the EDC model are different. The turbulent flame predicted by EDC is thinner and combustion is completed in a smaller domain than in the case of FGM.

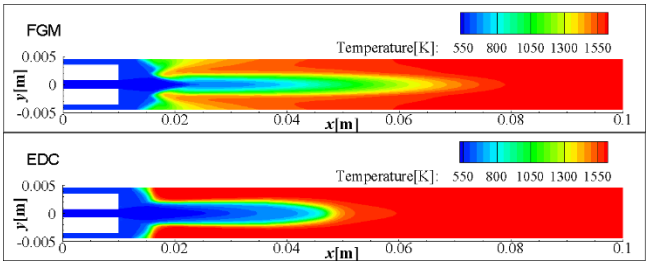

Fig. 2 Contours of mean temperature contours predicted by FGM and EDC (w_f=24 wt%, T_f=530 K)

Because in FGM the temperature is controlled by mixture fraction and progress variable, in order to understand the difference in temperature prediction it is necessary to retrieve the prediction of mixture fraction contained in the EDC model. The mean value of the unnormalized progress variable (mass fraction of CO_2) however is directly available in EDC. The mixture fraction can be obtained from the species

values according to equation (15). Because the relation between Z and the element mass fractions is linear and the boundary values are not fluctuating the same relation holds between mean values of Z and the element mass fractions.

Fig. 3 and Fig. 4 respectively show the contours of mean mixture fraction and mean progress variable. From Fig. 3 it is clear that EDC and FGM predict quite different mixing of fuel stream and oxidiser stream. The mean mixture fraction predicted by the EDC model become nearly evenly distributed at the axial positions larger than 0.03 m while the FGM model predicts that the mixing layer extends further downstream until axial position 0.07 m. In other words the mixing of fuel and oxidizer stream predicted by the EDC model is faster than that by the FGM model.

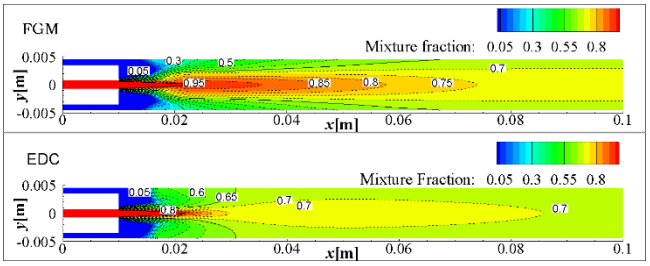

Fig. 3 Contours of mean mixture fraction contours by FGM and EDC (w_f=24 wt%, T_f=530 K)

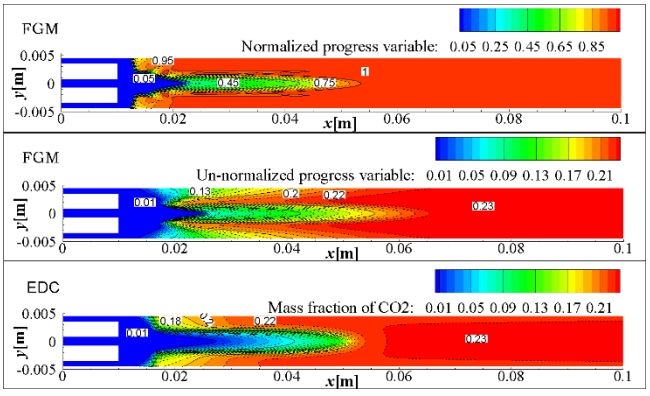

Fig. 4 Contours of mean progress variable by FGM and EDC (w_f=24 wt%, T_f=530 K)

In Fig. 4, the contours of normalized and un-normalized progress variable predicted by FGM and the mass fraction of CO_2 predicted by EDC are shown. The normalized progress variable represents the reaction progress at the local mixture

fraction but it is un-normalized progress variable, equal to the mass fraction of CO_2, that should be compared with the EDC prediction. The normalized progress variable reaches it maximal value one before the mixing of the fuel and oxidizer is reached, which means that the reaction has proceeded to the maximal extent at the corresponding mixture fraction and the reaction progress is limited by the mixing rate. From the analysis of the mixture fraction and progress variable contours, it can be concluded that the more extended flame predicted by the FGM model for Case 2 is mainly because of the slower mixing rate of fuel and oxidizer. In turbulent conditions, the species mixing is mainly controlled by the turbulent diffusion, which in RANS modeling is represented by the turbulent viscosity.

Fig. 5 shows the centerline profiles of turbulent viscosity and the mean temperature predicted by the two models. It shows that the maximum of the turbulent viscosity predicted by the FGM model is only half of that by the EDC model and the width of the peak in the profile by the FGM model is much smaller. The fact that the fast increase of mean temperature occurs at peak of the turbulent viscosity confirms that the reaction are fast and follow the mixing. The lower turbulent viscosity predicted by FGM model explains the slower temperature rise and the thicker flame. In order to understand why the turbulent viscosity profiles present such large difference, an analysis of the flow field predictions and the turbulence-chemistry interaction is needed.

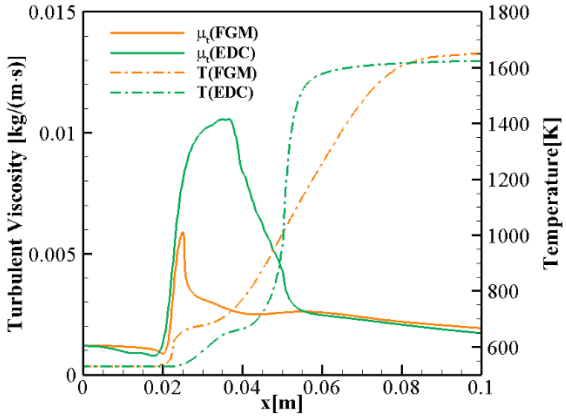

Fig. 5 Centerlines profile of turbulent viscosity and mean temperature (w_f=24 wt%, T_f=530 K)

3.2 Flow field analysis

The contours of mean velocity and turbulent viscosity predicted for the non-adiabatic case (case 1) and the adiabatic case (case 2) are displayed in Fig. 6 and Fig. 7 respectively. It shows that the inlet velocities of Case 1 (Fig. 6) are much higher than that of Case 2 (Fig. 7). This is due to the smaller density at higher inlet temperature (700 K, Case 1). Another difference between the two cases is that the velocity difference between the fuel and the oxidizer of Case 1 is larger than that of Case 2. This is because the density of oxygen is less sensitive to the temperature increase than the density of fuel. Due to the velocity difference between fuel and oxidizer, a recirculation zone is formed near the combustor wall, which is also observed by Narayanan et al. [14]. The recirculation zone of Case 1 is larger than that of Case 2, which can be explained by the Craya-Curtet relation [42-44] expressing that for a confined jet the length of the near wall recirculation zone increases with the velocity difference. Because of the higher velocity and velocity gradient, the turbulent viscosity of Case 1 is obviously larger than that of Case 2. This explains that the species mixing rate is not the limiting factor for Case 1 and why the difference in the

predicted flame length between the two models occurring in Case 2 is not observed in Case 1.

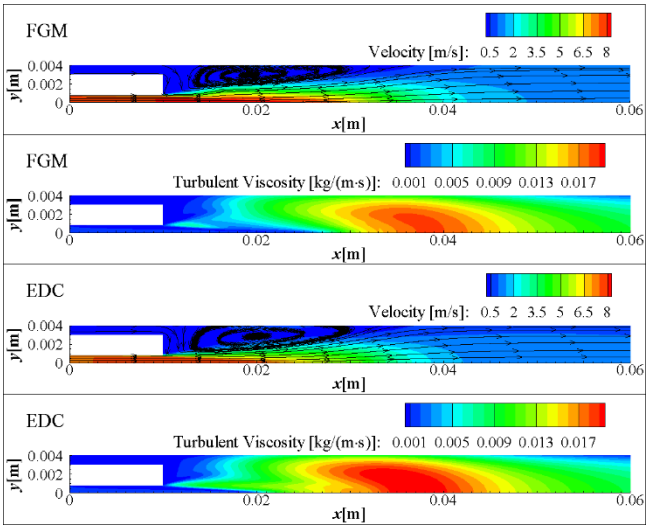

Fig. 6 Contours of mean velocity and turbulent viscosity for FGM and EDC (w_f=16 wt%, T_f=700 K).

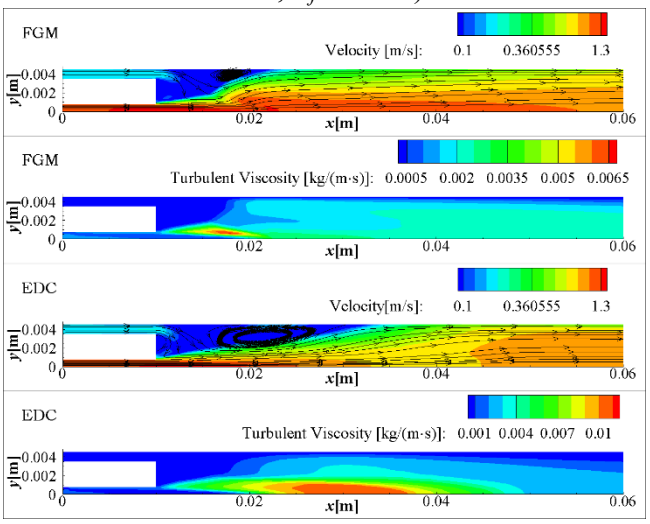

Fig. 7 Contours of mean velocity and turbulent viscosity for FGM and EDC (w_f=24 wt%, T_f=530 K).

The full contours of turbulent viscosity Case 2 predicted by FGM and EDC support the argument in *Section 3.1 Temperature profile* that the thicker flame predicted by the FGM model is due to the smaller turbulent viscosity. By analysing the velocity contours, we can explore which flow properties lead to the difference in turbulent viscosity profiles. In the flow field predicted by the FGM model, the velocity near the wall increases fast at the axial position around 0.02 m. As a result,

the velocity gradient in the downstream becomes smaller and so does the turbulent viscosity. Therefore, the FGM prediction of slow mixing rate in the downstream region is due to the rapid expansion in the upstream region. Essentially, the thicker flame predicted by the FGM model for the Case 2 is caused by the rapid reaction rate and temperature rise in the near nozzle zone. This is a clear indication that the differences between the predictions the FGM and EDC models come from the differences in turbulence-chemistry interaction modelling.

3.3 Turbulence-chemistry interaction

In this section we focus on the impact of the modelling of the mean chemical source term on the predictions. When the influence of turbulence is neglected, the reaction rates directly dependent on mean quantities (mass fractions and temperature), which is called “finite rate / no TCI”. In the EDC model and the FGM model, the TCI is represented in different ways, respectively given by Eq. 14 and Eq. 16. The finite rate / no TCI model can be directly considered as a limiting case of the EDC model because they solve for the same mean species mass fractions via transport equations. For the FGM model, the limiting case of no influence of turbulent fluctuations is the case where the PDF is not assumed to be a β-function but the rather a δ-function with the same mean but variance zero. It can easily be implemented by explicitly setting the variances of mixture fraction and progress variable to zero before looking up properties in the FGM table in the UDF file. To study the effect and importance of TCI now four models can be compared: FGM without TCI, finite rate / no TCI, FGM and EDC.

The mean source term of progress variable (the mass fraction of CO_2) predicted by these four models for the condition of adiabatic case (Case 2) are shown in Fig. 8. It is found that the source term contours calculated by the two models without TCI are

very similar. This proves that the chemistry reduction by the flamelet assumptions underlying the FGM approach is accurate. However, the source terms of EDC and FGM are clearly different. It can be concluded that it is not the chemistry reduction in FGM, but rather the different treatment of TCI that is the main source of difference between EDC and FGM with β-PDF. In the case of FGM including the influence of TCI makes the region where rapid reaction takes place move towards the nozzle while the maximum reaction rate is not much affected. In contrast, the in the case of EDC the zone with fast reaction moves downstream and the source term value is reduced by a factor five compared with the laminar reaction rate. It is also observed that in the case of FGM, with and without fluctuations, downstream of the main flame a weak secondary reaction zone appears.

It can be understood that the source term predicted by the EDC model is smaller than the laminar source term. In the EDC model at every time step the chemical state of the fine structure Y_i^* is recalculated starting from the current mean value $\tilde{Y}_i$ but the overall conversion is limited by the relaxation of $\tilde{Y}_i$ to the new value of Y_i^* by the time scale of mixing between the reacting structures and their surroundings. In contrast in the FGM model, the mean reaction rate is an average of many possibilities represented by the probability density function (PDF). Near the outlet of the nozzle, the reaction progress is at the beginning state and the laminar source term is quite small. The PDF integration of reaction source term in the whole *Z* and *c* range will lead to larger mean source term because any fluctuation in *Z* and *c* will both result in a larger source term compared with the minimum value. Hence, the TCI in FGM model accelerate the reaction rate in the near nozzle zone. The formulation using PDF integration is a richer representation of influence of spatial structure because the gradients of mean and variance of mixture fraction and progress variable play a key

role, not taken into account in the EDC model. Therefore, we consider the FGM results to be theoretically more accurate than the EDC ones. Nevertheless, more experimental data are needed to validate this.

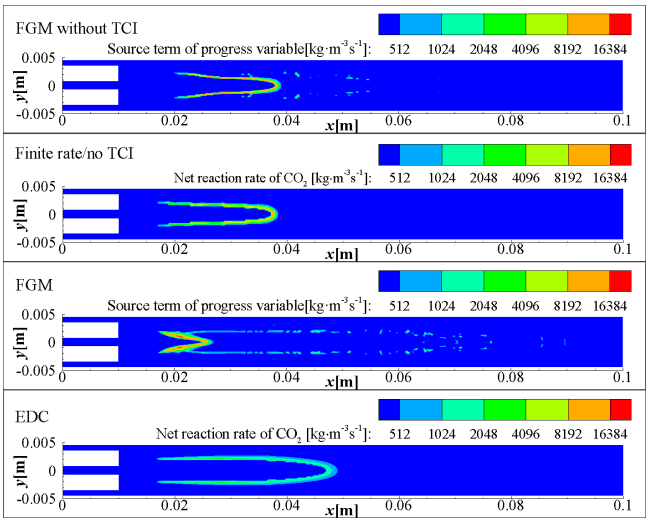

Fig. 8 Mean source term of progress variable for four different models: FGM without TCI, finite rate / no TCI, FGM and EDC (w_f=24 wt%, T_f=530 K)

3.4 Extinction limits

Avoiding extinction is a key objective in hydrothermal combustion. Extinction limits can be characterised by inlet temperature or mass flow rate. Extinction temperature is defined as the lowest inlet temperature that can sustain an flame [29] at fixed mass flow rate, extinction mass flow rate is the highest mass flow rate allowing a stable flame at constant inlet temperature. It should be noted that the term extinction here is used to denote absence of ignition. Extinction temperature, as defined above, can be relatively easy identified using the EDC model by doing a series of steady state simulations with a stepwise decreasing inlet temperature starting from a case with stable flame until the steady state turns into a state of mixing only. Using the FGM model the method of subsequent steady state calculations could be applied too, but a new table would have to be calculated for every step because the inlet temperatures are to be taken into account already in the counterflow laminar flame calculations.

Furthermore, the representation of the extinguished states (zero progress variable) and their probability becomes important. As has been discussed in our previous work [28], for a given inlet temperature and fuel concentration, the stability of the laminar flame is depending on the strain rate. For the turbulent flame, the probability of high strain rate is dependent on the flow conditions, which are influencing the profiles of mixture fraction, progress variable and their fluctuations. These are well-represented by the FGM method. Therefore, the FGM model is best suited to study the extinction mass flow rate other than the extinction temperature. Below we present results on extinction temperature obtained using EDC and results on extinction mass flow rate using both EDC and FGM.

Fig. 9, (a) to (c), present the profiles of mean temperature along the axis of the combustor for steady state operations with different inlet temperatures, for fuel concentration of 16 wt% (Case 3), 20 wt% (Case 4) and 24 wt% (Case5) respectively. Other boundary conditions including the mass flow rates are set to the experimental values listed in Table 1. The experimental extinction temperatures obtained by Wellig et al. [29] are 557 K (16 wt%), 513 K (20 wt%) and 460 K (24 wt%) respectively. From Fig. 9, it can be seen that with the decrease in inlet temperature, the flame temperature decreases and the axial position of maximum temperature moves downstream. When the inlet temperature decreases to 570 K and 410 K for the fuel concentration of 16 wt% and 20 wt% respectively, the maximum temperatures along the axis are only slightly higher than the inlet temperature. This indicates that the flames are already extinguished and the increase in temperature is just due to the mixing with the hot oxidizer. From this point of view, the extinction temperature predicted by the EDC model for Case 3 and Case 4 are 590 K and 430 K respectively, and that for Case 5 can be lower than the ambient temperature 300 K. These results

show considerable discrepancy with the experimental data. However, this can be explained by considering the length of the computational domain. In the simulation the combustor length was set to 0.1 m in order to avoid influence of outflow conditions on flame characteristics. However, the experimental combustor length is 0.06 m [29] which is denoted in Fig. 9. The experimental setup does not allow a flame at larger distance than 0.06 m. As described by Wellig et al. [29], the outside wall of the experimental combustor was surrounded by cooling water which mixed together with the outlet main flow from the combustor. Therefore, we can consider the modelling cases having the axial position of the maximum temperature larger than 0.06 m as actually representing experimental cases without flame. Taking this into account, the predicted extinction temperatures are 590 K (Case 3), 490 K (Case 4) and 450 K (Case 5), and the discrepancy with the experimental data is 33 K, 23 K and 10 K respectively. These results are significantly better than the ones obtained with the eddy dissipation / finite rate (ED/FR) model used in our previous work [17]. This is attributed mainly to the inclusion of detailed chemistry in the EDC model.

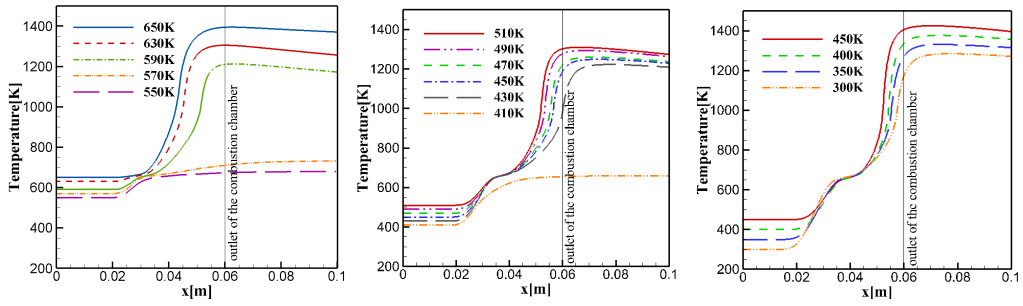

(a) w_f=16 wt% (b) w_f=20 wt% (c) w_f=24 wt%

Fig. 9 Centerline mean temperature profiles at different inlet temperature predicted by EDC model.

For the study of extinction mass flow rate, conditions with two different inlet temperatures have been studied, namely Case 6 and Case 7 (See Table 1). The fuel concentration of these cases is fixed as 24 wt%. Case 6 represents the highly stable conditions of which the inlet temperature (530 K of fuel) is much higher than the

extinction temperature, while Case 7 represents the critical conditions of which the inlet temperature (450 K of fuel) is very close to the extinction temperature. To identify the extinction mass flow rate from model predictions a series of steady state simulations have been done with different mass flow rate. The predicted temperature profiles revealing whether or not the steady state is a burning flame, are shown in Fig. 10 and Fig. 11. The f_{exp} in the legend denotes the experimental mass flow rate used in the experiments by Wellig et al. [29]. For Case 6, f_{exp} means 1.53 g/s of fuel and 0.65 g/s of oxidizer, while for Case 7, f_{exp} means 1.55 g/s of fuel and 0.65 g/s of oxidizer. The computed cases have mass flow rates equal to f_{exp} multiplying different integers from 1 to higher values until a state without flame is reached, as indicated. Three observations can be made on the results displayed in Fig. 10 and Fig. 11. Firstly, the extinction mass flow rates at higher inlet temperature are higher than that at lower inlet temperature. Secondly, the extinction mass flow rates predicted by the FGM model are significantly larger than that by the EDC model. Thirdly, the temperature profiles predicted by the FGM model cross with each other, while that by the EDC model do not.

The first observation explained by the fact that at higher inlet temperature, the ignition proceeds more quickly and the flame temperature is higher, both contributing to shift of the blow-off limit to higher mass flow rates. To explain the second and the third observations more analysis is needed. As discussed in the previous sections, the slower mixing rate is the main reason that leads to the difference in flame structure predicted by the FGM model compared to that by the EDC model for Case 2, which is equally to the f_{exp} condition of Case 6. With the increase in the inlet mass flow rate, the turbulent intensity increases and the mixing rate of the fuel and oxidizer is accelerated. As a result, the mixing-controlled flame region, which is characterized by

the relative slow temperature rise in Fig. 10 (b), narrows down from the condition of f_{exp} to the condition of $10f_{exp}$. When the inlet mass flow rates increase to 50 times of the experimental values ($50f_{exp}$), the two-region temperature rising feature disappears and the flame thickness reaches the minimum. This explains the cross of the temperature profiles by the FGM model. From this point of view, by the FGM model, moderate increase in the inlet mass flow rates improves the flame stability, unlike that by the EDC model, the increase in mass flow rates monotonously push the flame to the downstream until blow-off. This results that the extinction mass flow rates predicted by the FGM model are larger than that by the EDC model. The inherent reason of this difference is still the different treatment of the turbulence-chemistry interaction, discussed in *Section 3.3 Turbulence-chemistry interaction*. The results here show that the extinction limit as function of mass flow rate is not obvious and they call for further experimental research. This limit would be a key factor to determine the boundaries of stable operation in industrial hydrothermal combustor design.

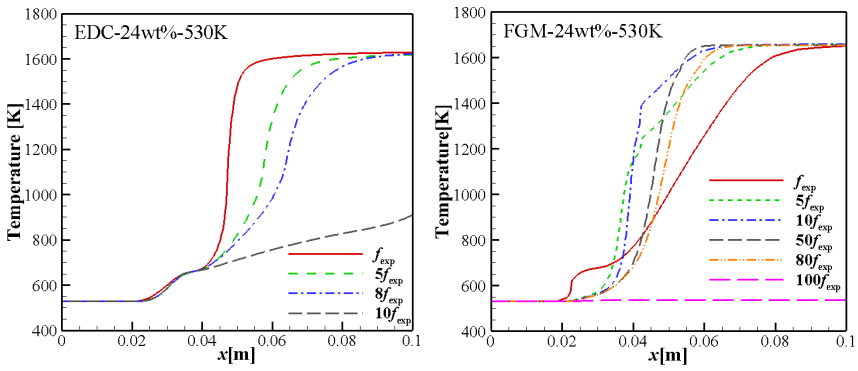

(a) EDC (b) FGM

Fig. 10 Centerline profile of mean temperature at different mass flow rates, predicted by EDC and FGM models (w_f=24 wt%, T_f=530 K)

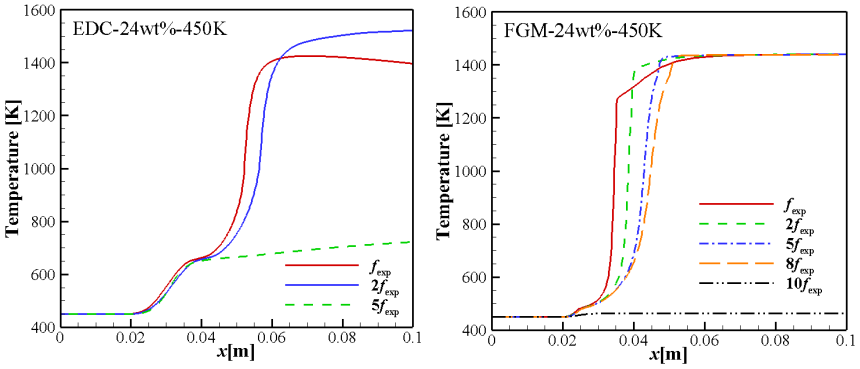

(a) EDC (b) FGM

Fig. 11 Center line profile of mean temperature at different mass flow rates, predicted by EDC and FGM models (w_f=24 wt%, T_f=450 K)

4 Conclusion

The eddy dissipation concept (EDC) model and the flamelet generated manifolds (FGM) model have both been successfully applied to the simulation of turbulent methanol hydrothermal combustion in the experimental setup of ETH. In both modelling approaches appropriate real-fluid properties were used. FGM tables have been generated by a modified version of CHEM1D, used earlier for calculation of laminar hydrothermal flames, but extended with a PDF model for turbulence-chemistry interaction. Since the heat loss effect has not been included in the FGM tables, the present FGM model can only predict the adiabatic conditions.

At supercritical inlet temperature (700 K, Case1) EDC and FGM predict similar profiles of centreline mean temperature, but also taking into account the spatial resolution of the thermocouple data, the FGM model is found to be more representing the initial rise of mean temperature. At subcritical inlet temperature (530 K, Case2), the flame predicted by the FGM model is thicker than that by the EDC model, which is directly caused by the slower mixing rate predicted by the FGM model. Analysis on the flow fields make clear that the different density and velocity variations caused by

the different reaction and heat release rate are the main reason that lead to the different turbulent mixing rate.

The EDC model is able to predict the extinction temperatures with a deviation of only 10K to 33 K, which is significantly better than previous modelling results on this flame in literatures. Extinction mass flow rates are predicted for the first time. They are considered to be a key factor for scale-up design of industrial hydrothermal combustors. The extinction mass flow rates predicted by the FGM model are higher than that by the EDC model. Results by the FGM model indicate that the increase in mass flow rate first improves the flame stability and then, after further increase, blows off the flame, while the improvement of stability by increasing mass flow rate is not observed by the EDC model.

Analysis of the reaction source terms by the two models and their laminar versions indicate that the effect of turbulence on the reaction rate by the FGM model is positive near the nozzle and negative in the downstream zone while that by the EDC model is always negative. This essential difference caused by the different representation of the turbulence-chemistry interactions explains all the differences between the predictions by the two models. Theoretically, the results by the FGM model (combined with a PDF model) are expected to be more accurate because of the explicit modelling of the characteristics of turbulent fluctuations (variances of mixture fraction and progress variable). Nevertheless, more experimental data are needed to validate it.

Acknowledgements

The authors thank the China scholarship council (CSC) for financial support for the first author.

References

[1] C. Augustine, J.W. Tester, Hydrothermal flames: From phenomenological experimental demonstrations to quantitative understanding, J. Supercrit. Fluids, 47 (2009) 415-430.https://doi.org/10.1016/j.supflu.2008.10.003

[2] D.S. Gokkaya, M. Sert, M. Saglam, M. Yuksel, L. Ballice, Hydrothermal gasification of the isolated hemicellulose and sawdust of the white poplar (Populus alba L.), J. Supercrit. Fluids, 162 (2020).http://dx.doi.org/10.1016/j.supflu.2020.104846

[3] Y. Hu, L. Qi, K.T.V. Rao, B. Zhao, H. Li, Y. Zeng, C. Xu, Supercritical water gasification of biocrude oil from low-temperature liquefaction of algal lipid extraction residue, Fuel, 276 (2020).http://dx.doi.org/10.1016/j.fuel.2020.118017

[4] H. Jin, B. Bai, W. Wei, Y. Chen, Z. Ge, J. Shi, Hydrothermal Liquefaction of Polycarbonate (PC) Plastics in Sub-/ Supercritical Water and Reaction Pathway Exploration, ACS Sustainable Chem. Eng., 8 (2020) 7039-7050.http://dx.doi.org/10.1021/acssuschemeng.0c00700

[5] C. Yang, S.Z. Wang, M.M. Ren, Y.H. Li, W.H. Song, Hydrothermal Liquefaction of an Animal Carcass for Biocrude Oil, Energy & Fuels, 33 (2019) 11302-11309.http://dx.doi.org/10.1021/acs.energyfuels.9b03100

[6] A. Kruse, E. Dinjus, Hot compressed water as reaction medium and reactant: Properties and synthesis reactions, J. Supercrit. Fluids, 39 (2007) 362-380.http://dx.doi.org/10.1016/j.supflu.2006.03.016

[7] Y. Takahashi, Y. Nakayasu, K. Iwase, H. Kobayashi, I. Honma, Supercritical hydrothermal synthesis of MoS2 nanosheets with controllable layer number and phase structure, Dalton Transactions, 49 (2020) 9377-9384.http://dx.doi.org/10.1039/d0dt01453b

[8] M.D. Bermejo, P. Cabeza, J.P.S. Queiroz, C. Jimenez, M.J. Cocero, Analysis of the scale up of a transpiring wall reactor with a hydrothermal flame as a heat source for the supercritical water oxidation, J. Supercrit. Fluids, 56 (2011) 21-32.https://doi.org/10.1016/j.supflu.2010.11.014

[9] Z. Yan, B. Ormeci, Y. Han, J. Zhang, Supercritical water oxidation for treatment of wastewater sludge and recalcitrant organic contaminants, Environmental Technology & Innovation, 18 (2020).http://dx.doi.org/10.1016/j.eti.2020.100728

[10] L.L. Qian, S.Z. Wang, M.M. Ren, S. Wang, Co-oxidation effects and mechanisms between sludge and alcohols (methanol, ethanol and isopropanol) in supercritical water, Chem. Eng. J, 366 (2019) 223-234.https://doi.org/10.1016/j.cej.2019.02.046

[11] M. Jose Cocero, Supercritical water processes: Future prospects, J. Supercrit. Fluids, 134 (2018) 124-132.http://dx.doi.org/10.1016/j.supflu.2017.11.018

[12] J.P.S. Queiroz, M.D. Bermejo, F. Mato, M.J. Cocero, Supercritical water oxidation with hydrothermal flame as internal heat source: Efficient and clean energy production from waste, J. Supercrit. Fluids, 96 (2015) 103-113.https://doi.org/10.1016/j.supflu.2014.09.018

[13] P. Cabeza, J.P. Silva Queiroz, M. Criado, C. Jimenez, M. Dolores Bermejo, F. Mato, M. Jose Cocero, Supercritical water oxidation for energy production by hydrothermal flame as internal heat source. Experimental results and energetic study, Energy, 90 (2015) 1584-1594.https://doi.org/10.1016/j.energy.2015.06.118
[14] C. Narayanan, C. Frouzakis, K. Boulouchos, K. Príkopský, B. Wellig, P. Rudolf von Rohr, Numerical modelling of a supercritical water oxidation reactor containing a hydrothermal flame, J. Supercrit. Fluids, 46 (2008) 149-155.https://doi.org/10.1016/j.supflu.2008.04.005
[15] J. Sierra-Pallares, M. Teresa Parra-Santos, J. García-Serna, F. Castro, M. José Cocero, Numerical modelling of hydrothermal flames. Micromixing effects over turbulent reaction rates, J. Supercrit. Fluids, 50 (2009) 146-154..https://doi.org/10.1016/j.supflu.2009.05.001
[16] J.P.S. Queiroz, M.D. Bermejo, M.J. Cocero, Numerical study of the influence of geometrical and operational parameters in the behavior of a hydrothermal flame in vessel reactors, Chem. Eng. Sci., 112 (2014) 47-55.https://doi.org/10.1016/j.ces.2014.03.019
[17] M.M. Ren, S.Z. Wang, C. Yang, Ignition and Extinction Modeling of Hydrothermal Flames, in: H. Hou, Z. Han (Eds.) Proceedings of the 2017 5th International Conference on Machinery, Materials and Computing Technology, Atlantis Press, Paris, 2017, pp. 439-443.https://doi.org/10.2991/icmmct-17.2017.93
[18] P.S. Veloo, Y.L. Wang, F.N. Egolfopoulos, C.K. Westbrook, A comparative experimental and computational study of methanol, ethanol, and n-butanol flames, Combust. Flame, 157 (2010) 1989-2004.https://doi.org/10.1016/j.combustflame.2010.04.001
[19] H. Wang, R. Xu, K. Wang, C.T. Bowman, R.K. Hanson, D.F. Davidson, K. Brezinsky, F.N. Egolfopoulos, A physics-based approach to modeling real-fuel combustion chemistry - I. Evidence from experiments, and thermodynamic, chemical kinetic and statistical considerations, Combust. Flame, 193 (2018) 502-519.http://dx.doi.org/10.1016/j.combustflame.2018.03.019
[20] S. Taileb, J. Melguizo-Gavilanes, A. Chinnayya, Influence of the chemical modeling on the quenching limits of gaseous detonation waves confined by an inert layer, Combust. Flame, 218 (2020) 247-259.http://dx.doi.org/10.1016/j.combustflame.2020.04.018
[21] A. De, E. Oldenhof, P. Sathiah, D. Roekaerts, Numerical Simulation of Delft-Jet-in-Hot-Coflow (DJHC) Flames Using the Eddy Dissipation Concept Model for Turbulence–Chemistry Interaction, Flow, Turbulence and Combustion, 87 (2011) 537-567.https://doi.org/10.1007/s10494-011-9337-0
[22] M.J. Evans, P.R. Medwell, Z.F. Tian, Modeling lifted jet flames in a heated coflow using an optimized eddy dissipation concept model, Combust Sci Technol, 187 (2015) 1093-1109.https://doi.org/10.1080/00102202.2014.1002836
[23] N. Romero-Anton, X. Huang, H. Bao, K. Martin-Eskudero, E. Salazar-Herran, D. Roekaerts, New extended eddy dissipation concept model for flameless combustion in furnaces, Combust. Flame, 220 (2020) 49-62.https://doi.org/10.1016/j.combustflame.2020.06.025

[24] J.A. van Oijen, A. Donini, R.J.M. Bastiaans, J.H.M. ten Thije Boonkkamp, L.P.H. de Goey, State-of-the-art in premixed combustion modeling using flamelet generated manifolds, Progress in Energy and Combustion Science, 57 (2016) 30-74.https://doi.org/10.1016/j.pecs.2016.07.001
[25] M.U. Göktolga, J.A. van Oijen, L.P.H. de Goey, Modeling MILD combustion using a novel multistage FGM method, Proc. Combust. Inst., 36 (2017) 4269-4277.https://doi.org/10.1016/j.proci.2016.06.004
[26] M. Ihme, C.M. Cha, H. Pitsch, Prediction of local extinction and re-ignition effects in non-premixed turbulent combustion using a flamelet/progress variable approach, Proc. Combust. Inst., 30 (2005) 793-800.https://doi.org/10.1016/j.proci.2004.08.260
[27] A. Parente, M.R. Malik, F. Contino, A. Cuoci, B.B. Dally, Extension of the eddy dissipation concept for turbulence/chemistry interactions to MILD combustion, Fuel, 163 (2016) 98-111.https://doi.org/10.1016/j.fuel.2015.09.020
[28] M.M. Ren, S.Z. Wang, D. Roekaerts, Numerical study of the counterflow diffusion flames of methanol hydrothermal combustion: The real-fluid effects and flamelet analysis, J. Supercrit. Fluids, 152 (2019) 104552.https://doi.org/10.1016/j.supflu.2019.104552
[29] B. Wellig, M. Weber, K. Lieball, K. Príkopský, P. Rudolf von Rohr, Hydrothermal methanol diffusion flame as internal heat source in a SCWO reactor, J. Supercrit. Fluids, 49 (2009) 59-70
[30] K. Príkopský, Characterization of continuous diffusion flames in supercritical water, in: Doctor of Technical Sciences Thesis, Swiss Federal Institute of Technology, Zurich, 2007.http://dx.doi.org/10.3929/ethz-a-005509478
[31] T. Poinsot, D. Veynante, Theoretical and numerical combustion, R.T. Edwards, Inc, Philadelphia, PA, 2005
[32] M.M. Ren, S.Z. Wang, J. Zhang, Y. Guo, D. Xu, Y. Wang, Characteristics of Methanol Hydrothermal Combustion: Detailed Chemical Kinetics Coupled with Simple Flow Modeling Study, Ind. Eng. Chem. Res., 56 (2017) 5469-5478.http://dx.doi.org/10.1021/acs.iecr.7b00886
[33] J. Li, Z. Zhao, A. Kazakov, M. Chaos, F.L. Dryer, J.J. Scire, A comprehensive kinetic mechanism for CO, CH2O, and CH3OH combustion, International Journal of Chemical Kinetics, 39 (2007) 109-136
[34] R.W. Bilger, S.H. Stårner, R.J. Kee, On reduced mechanisms for methane air combustion in nonpremixed flames, Combust. Flame, 80 (1990) 135-149.https://doi.org/10.1016/0010-2180(90)90122-8
[35] X. Huang, Measurements and model development for flameless combustion in a lab-scale furnace, in, Delft University of Technology, Delft, 2018,
[36] B. Marracino, D. Lentini, Radiation Modelling in Non-Luminous Nonpremixed Turbulent Flames, Combust Sci Technol, 128 (1997) 23-48.https://doi.org/10.1080/00102209708935703
[37] M. Stöllinger, D. Roekaerts, PDF modelling of soot formation in turbulent non-premixed flames using tabulated chemistry, in: Proceedings of the European Combustion Meeting, 2013,

[38] G. Frank, M. Pfitzner, On the Generation of Non-Adiabatic, Non-Premixed Flamelet Libraries with special emphasis on Wall Heat Losses, in: 9th Mediterranean Combustion Symposium, 2015,
[39] M.C. Hicks, U.G. Hegde, J.J. Kojima, Hydrothermal ethanol flames in Co-flow jets, J. Supercrit. Fluids, 145 (2019) 192-200.https://doi.org/10.1016/j.supflu.2018.12.010
[40] S.N. Reddy, S. Nanda, P. Kumar, M.C. Hicks, U.G. Hegde, J.A. Kozinski, Impacts of oxidant characteristics on the ignition of n-propanol-air hydrothermal flames in supercritical water, Combust. Flame, 203 (2019) 46-55.https://doi.org/10.1016/j.combustflame.2019.02.004
[41] P. Stathopoulos, K. Ninck, P.R. von Rohr, Hot-wire ignition of ethanol-oxygen hydrothermal flames, Combust. Flame, 160 (2013) 2386-2395.https://doi.org/10.1016/j.combustflame.2013.05.006
[42] R. Curtet, Confined jets and recirculation phenomena with cold air, Combust. Flame, 2 (1958) 383-411.https://doi.org/10.1016/0010-2180(58)90032-4
[43] H.F. Elattar, R. Stanev, E. Specht, A. Fouda, CFD simulation of confined non-premixed jet flames in rotary kilns for gaseous fuels, Computers & Fluids, 102 (2014) 62-73.https://doi.org/10.1016/j.compfluid.2014.05.033
[44] A. Revuelta, C. Martinez-Bazan, A.L. Sanchez, A. Linan, Laminar Craya-Curtet jets, Physics of Fluids, 16 (2004) 208-211.https://doi.org/10.1063/1629300